Supporting Information

Ultrahigh capacity and cyclability of dual-phase TiO$_2$ nanowires with low working potential at room and subzero temperatures

Dongmei Lin, [a] Linlong Lyu, [a] Kaikai Li, [b,*] Guohua Chen, [a] Haimin Yao, [a] Feiyu Kang, [c] Baohua Li, [c,*] Limin Zhou [d*]

[a] Department of Mechanical Engineering, The Hong Kong Polytechnic University, Hong Kong, China

[b] School of Materials Science and Engineering, Harbin Institute of Technology, Shenzhen, China

[c] Shenzhen Key Laboratory of Power Battery Safety and Shenzhen Geim Graphene Center, Graduate School at Shenzhen, Tsinghua University, Shenzhen, 518055, China
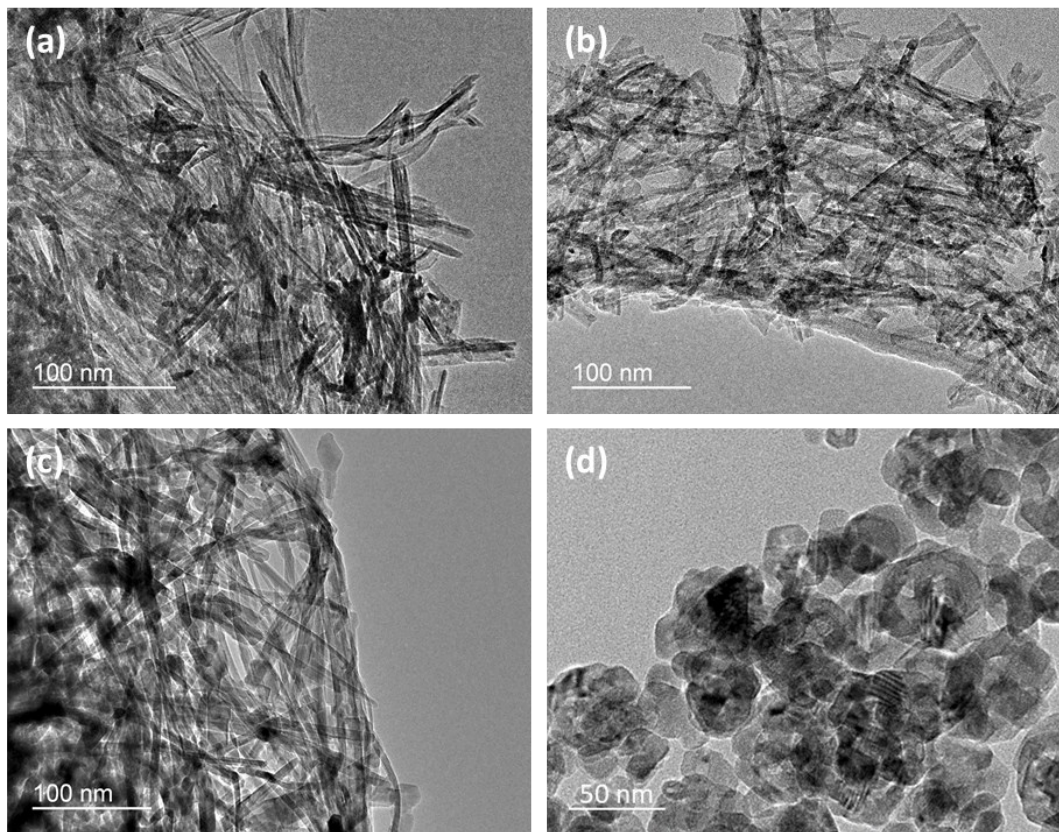
[d] School of System Design and Intelligent Manufacturing, Southern University of Science and Technology, Shenzhen, China
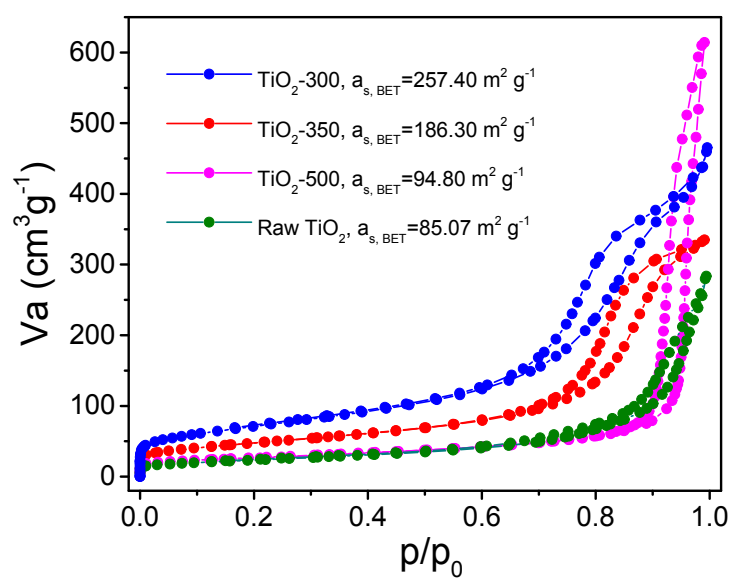
Corresponding authors:

E-mail address: zhoulm@sustech.edu.cn (L. Zhou)

E-mail address: likaikai@hit.edu.cn (K. Li)

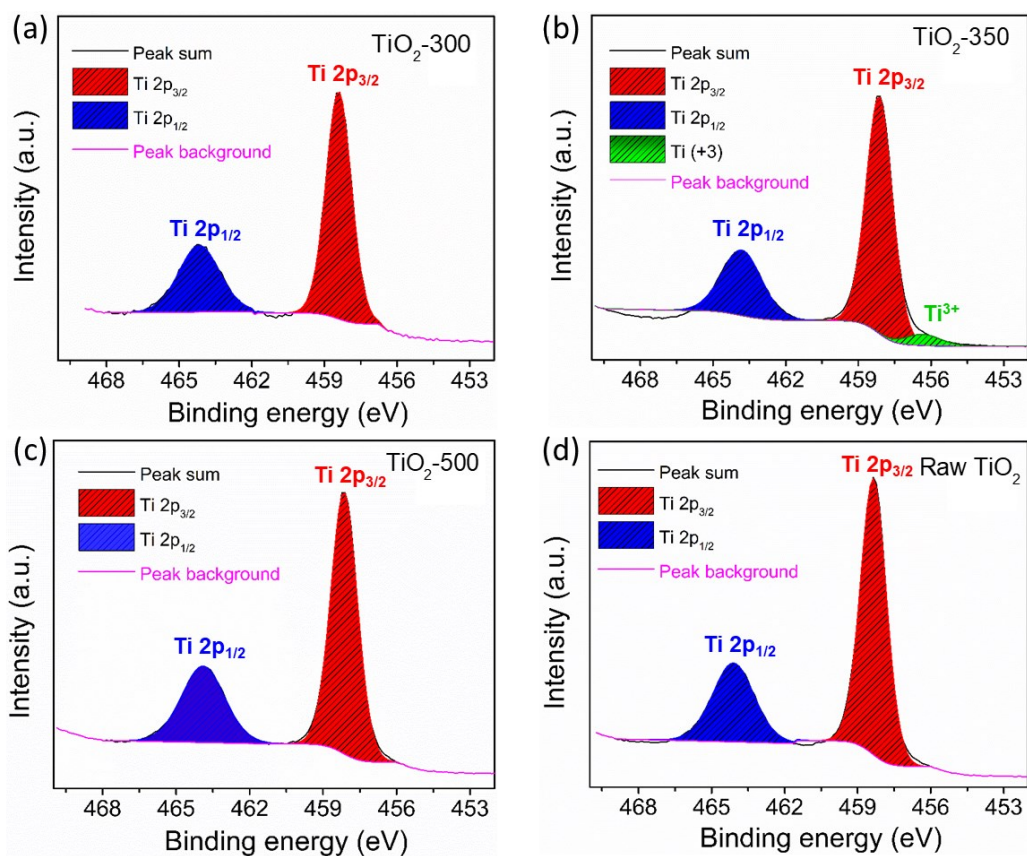E-mail address: libh@sz.tsinghua.edu.cn (B. Li)

Fig. S1. TEM images of TiO_2-300, TiO_2-350, TiO_2-500 nanowires, and raw TiO_2 nanoparticles, respectively.
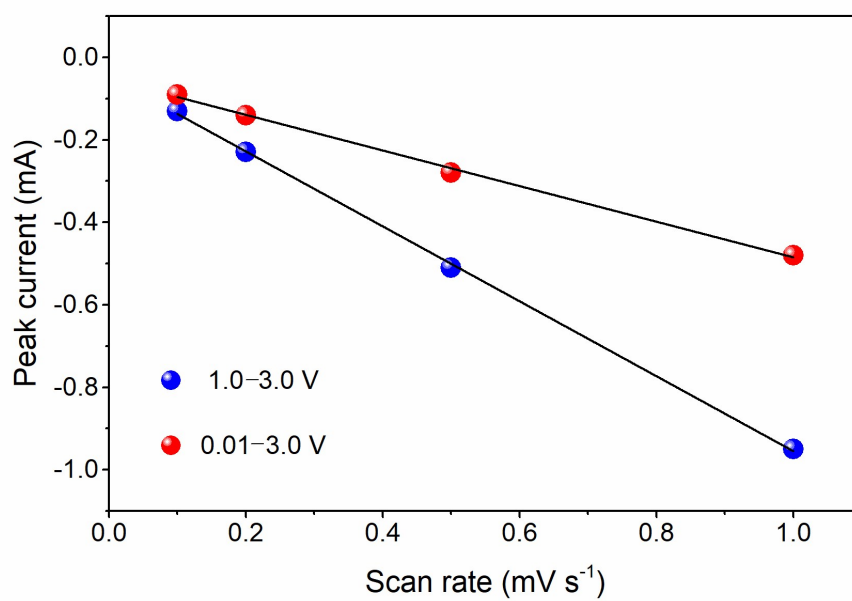

Fig. S2. Nitrogen adsorption/desorption isotherms of TiO_2-300, TiO_2-350, TiO_2-500, and raw TiO_2 nanoparticles, respectively.
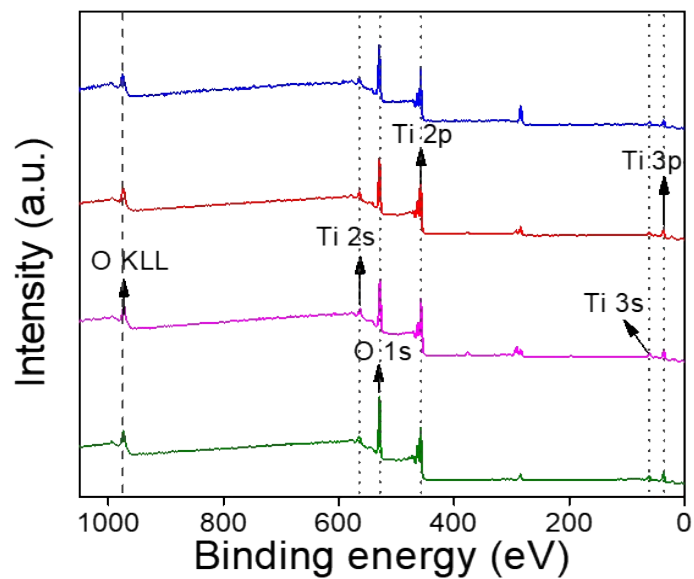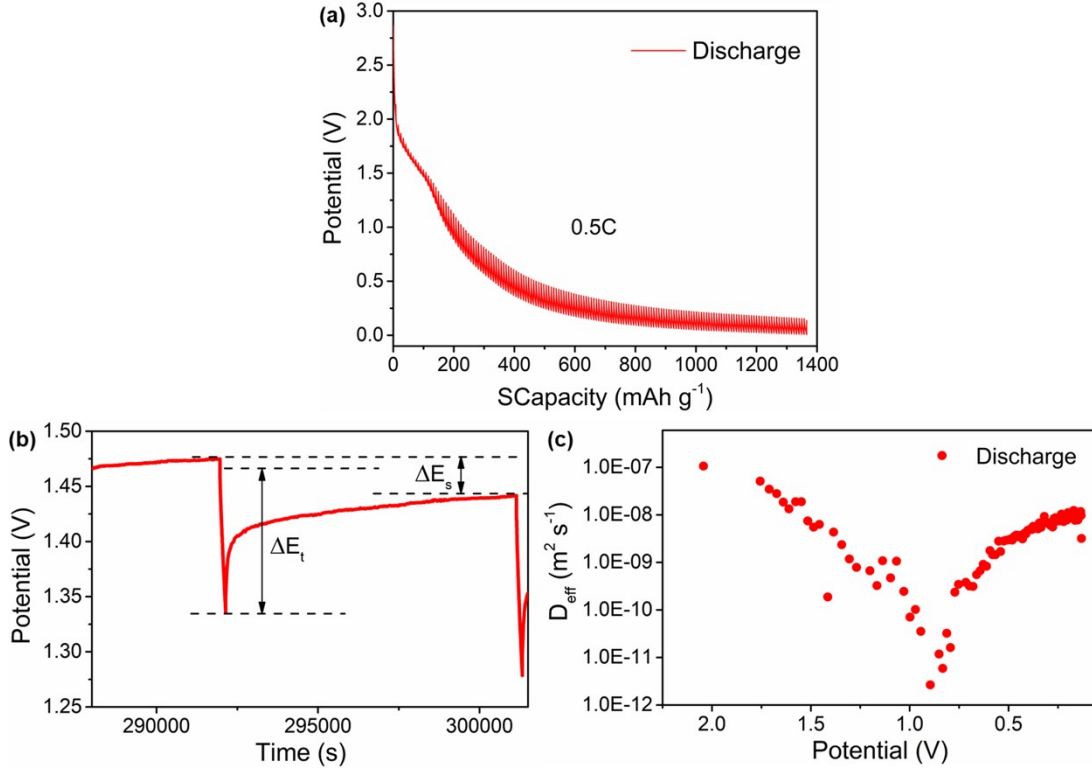
Fig. S3. XPS spectra of TiO_2-300, TiO_2-350, TiO_2-500, and raw TiO_2 nanoparticles, respectively.

Fig. S4. XPS Ti 2p spectra of (a) TiO_2-300, (b) TiO_2-350, (c) TiO_2-500 nanowires, and (d) raw TiO_2 nanoparticles.

Fig. S5. The relationship between the peak current and the scan rate of the TiO$_2$-B phase in the TiO$_2$-350 anode in the two potential windows.

Fig. S6. (a) GITT voltage profiles and equilibrium potentials during discharge in the enlarged potential window at 0.5C rate. (b) Voltage profile for a single titration of the GITT during discharge. (c) The apparent Li diffusion coefficient D_{app} at various states of discharge determined from the GITT voltage profiles.

We calculated the apparent Li diffusion coefficients D_{app} by assuming that Li^+ diffusion obeys Fick's second law:

$$D_{app} = \frac{4}{\pi\tau}\left(\frac{m_B V_M}{M_B S}\right)^2 \left(\frac{\Delta E_s}{\Delta E_t}\right)^2$$

(1)

where τ donates current pulse time, m_B, V_M, and M_B are the mass, molar volume and atomic weight of the electrode material TiO_2, respectively, and S presents the total contact area between the electrolyte and the electrode.

Before the GITT measurement, the cell was galvanostatic cycled at 0.5 C for 5 cycles between 0.01 V to 3 V.

During the GITT measurement, the cell was discharged at the rate of 0.5C (1 C = 335 mA g^{-1}) for 3 min, then followed by a relaxation for 150 min to reach the steady-state voltages. The potential window of GITT measurement ranges from 0.01 V to 3 V.
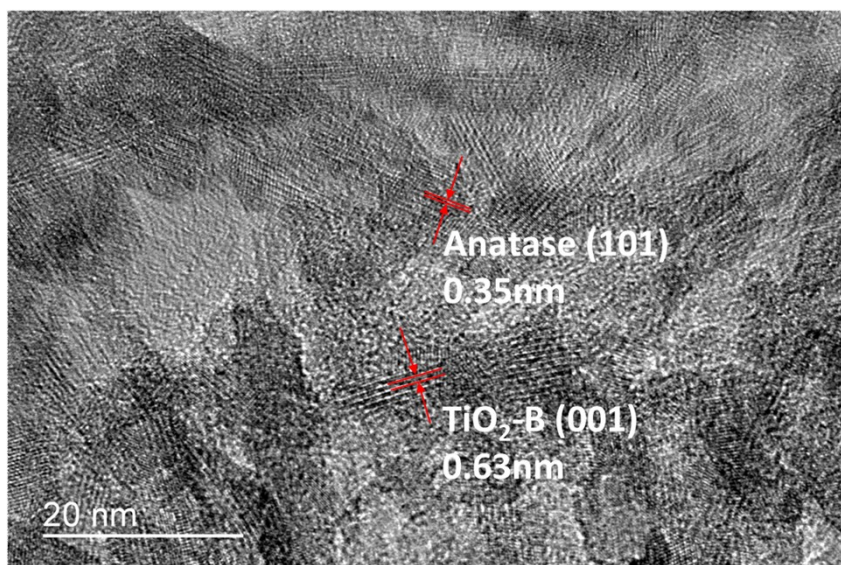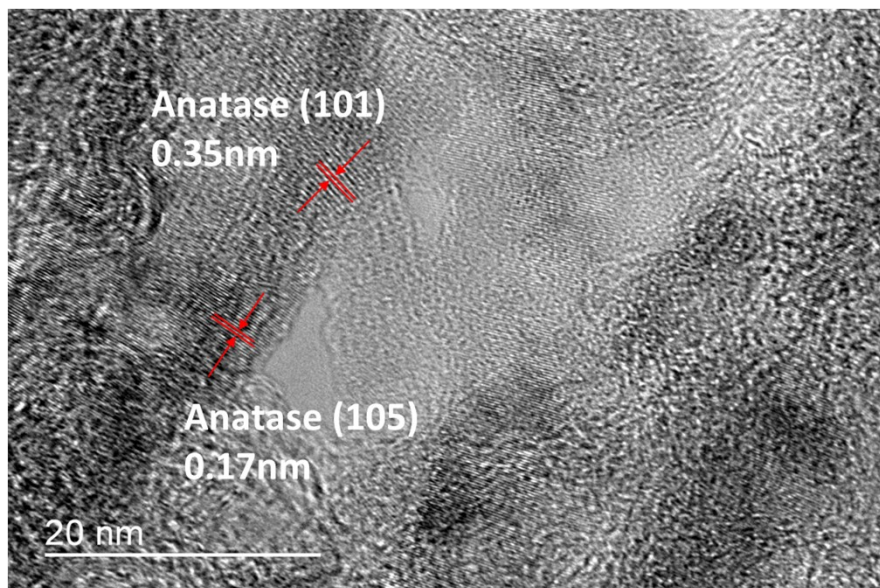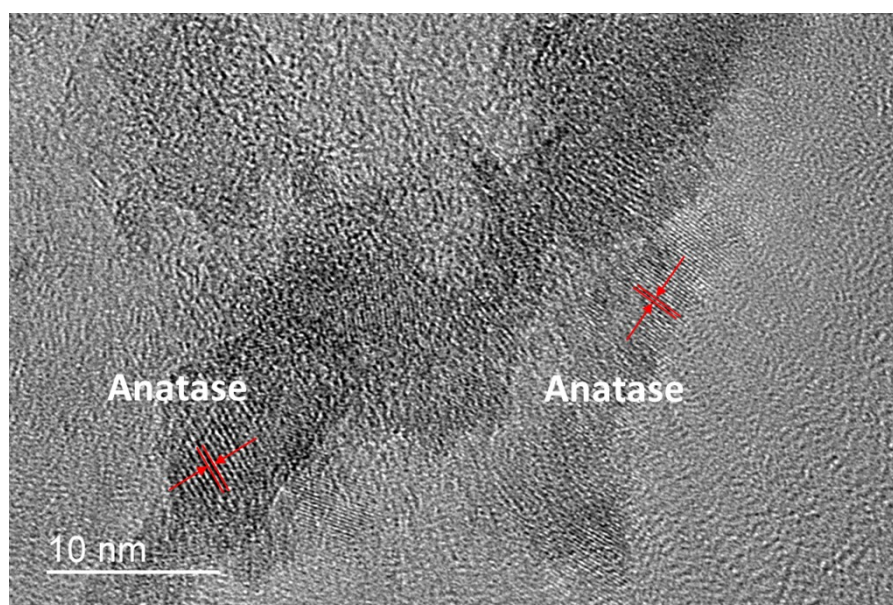
Fig. S7. HRTEM image of the TiO$_2$-350 anode discharged from OCP to 1.0 V.
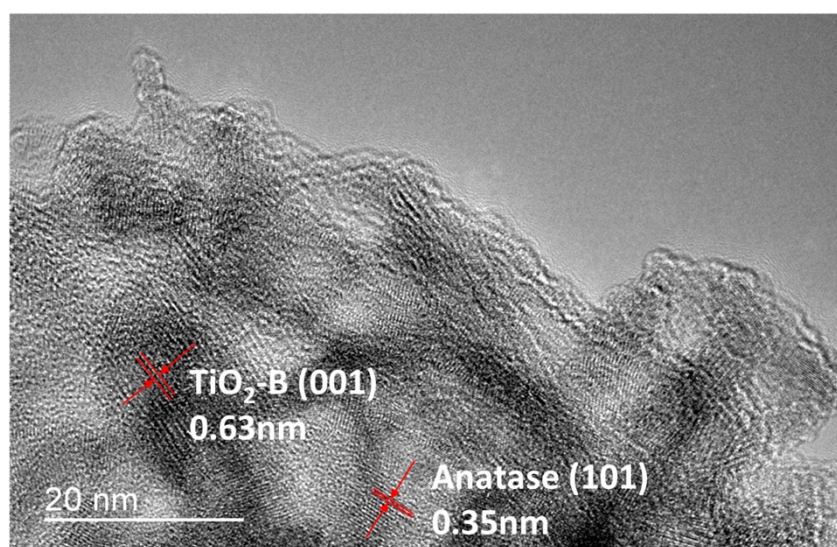
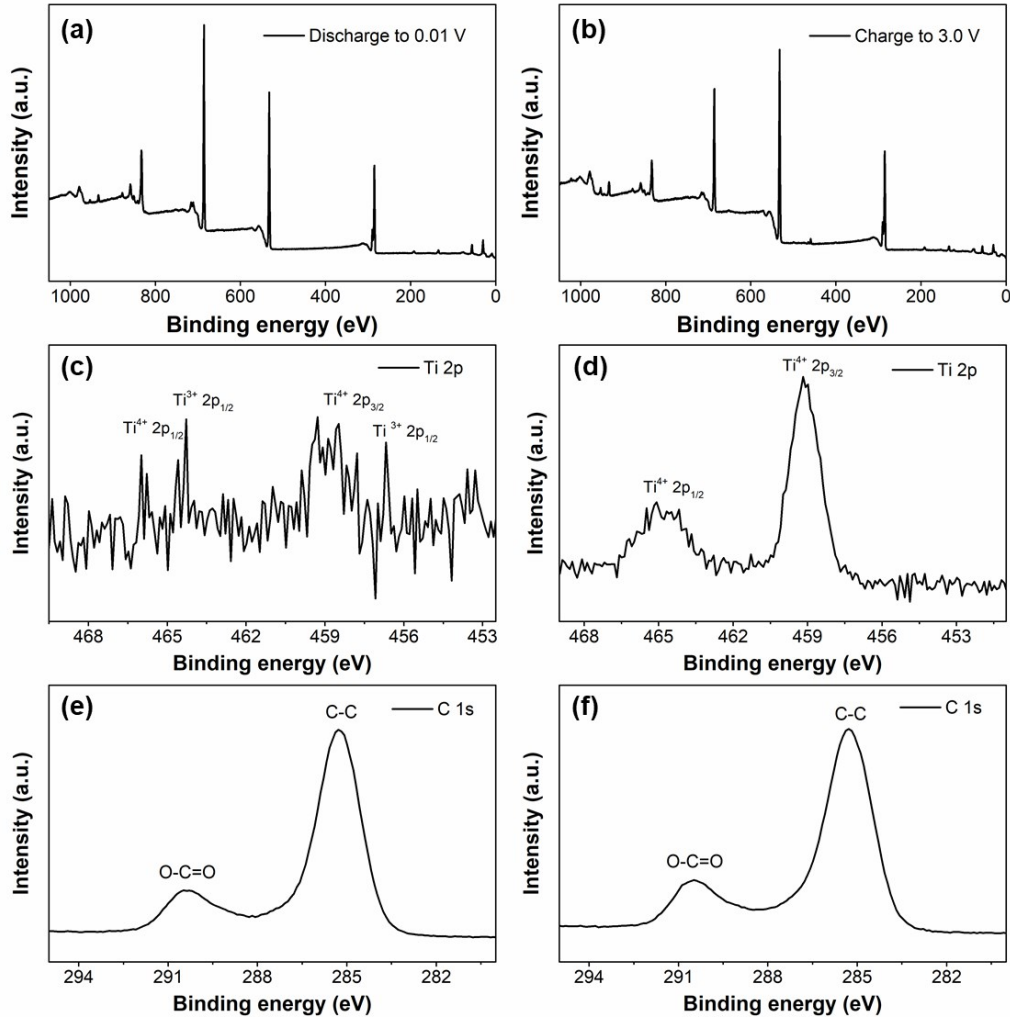**Fig. S8.** HRTEM image of the TiO$_2$-350 anode discharged from OCP to 0.5 V.

Fig. S9. HRTEM image of the TiO$_2$-350 anode after cycling 100 cycles in the potential window of 0.01–3.0 V.

Fig. S10. HRTEM image of the TiO$_2$-350 anode after cycling 500 cycles in the potential window of 0.01–3.0 V.

Fig. S11. Ex-situ XPS spectra of the TiO_2-350 anode when (a) discharged to 0.01 V, and (b) charged to 3.0 V. High resolution spectra of Ti element when (c) discharged to 0.01 V, and (d) charged to 3.0 V, and high resolution spectra of C element when (e) discharged to 0.01 V, and (f) charged to 3.0 V, respectively.

Ex-situ XPS results show that the typical Ti^{4+} $2p_{1/2}$ and Ti^{4+} $2p_{3/2}$ peaks significantly diminish while Ti^{3+} $2p_{3/2}$ peak appears after discharging to 0.01 V, indicating the reduction of Ti^{4+} to Ti^{3+} which accounts for the ultrahigh capacity. When charging to 3.0 V, the characteristic Ti^{3+} $2p_{3/2}$ peak disappears while both Ti^{4+} $2p_{1/2}$ and Ti^{4+} $2p_{2/3}$ peaks recover. In addition, there is no other side reaction like formation of Ti-C bonding occurs during charging/discharging process. However, even assuming that all Ti^{4+} ions reduce into Ti^{3+} in the discharging process, this cannot contribute to such high capacity. Furthermore, it does not occur the reduction of Ti^{4+} to Ti^0 at the end of discharging, indicating that the additional capacity is also not from the conversion reaction of Ti^{4+} to Ti^0. Herein, we propose that the additional capacity mainly derives from two parts: the intercalation lithiation and surface/interface Li ion storage behavior in the dual-phase TiO_2 nanowires.

Table S1. Initial CEs of anodes in the two potential windows of 1.0–3.0 V and 0.01–3.0 V, respectively.

Anodes	Initial CEs in the potential window of 1.0–3.0 V (%)	Initial CEs in the potential window of 0.01–3.0 V (%)
TiO$_2$–300	33.03	31.51
TiO$_2$–350	32.25	30.52
TiO$_2$–500	36.31	33.56
Raw TiO$_2$	33.86	34.83

References

1   W. Weppner and R. A. Huggins, J. Electrochem. Soc., 1977, 124, 1569-1578.